RSC Advances

ROYAL SOCIETY OF CHEMISTRY

PAPER

View Article Online
View Journal | View Issue

Check for updates

Cite this: *RSC Adv.*, 2023, **13**, 31528

Study on the behavior and mechanism of NiFe-LDHs used for the degradation of tetracycline in the photo-Fenton process†

Xia Liu,‡ Yuting Zhou,‡ Shuanghui Sun and Siqi Bao *

Received 12th August 2023
Accepted 14th October 2023

DOI: 10.1039/d3ra05475f

rsc.li/rsc-advances

An environment-friendly 3D NiFe-LDHs photocatalyst was fabricated *via* a simple hydrothermal method and characterized by means of SEM, XRD, BET, XPS and FT-IR. It is a highly efficient heterogeneous photo-Fenton catalyst for the degradation of TC-HCl under visible light irradiation. After exploring the effects of catalyst dosage, initial concentration of TC-HCl, solution pH and H_2O_2 concentrations, the optimal reaction conditions were determined. The experiment results showed that the degradation efficiency can reach 99.11% through adding H_2O_2 to constitute a photo-Fenton system after adsorption for 30 min and visible light for 60 min. After four cycles, the degradation rate decay is controlled within 21.2%, indicating that NiFe-LDHs have excellent reusable performance. The experimental results of environmental factors indicate that Fe^{2+} and Ca^{2+} promoted the degradation of TC-HCl, both Cl^- and CO_3^{2-} inhibited the degradation of TC-HCl. Two other antibiotics (OTC and FT) were selected for research and found to be effectively removed in this system, achieving effective degradation of a variety of typical new pollutants. The radical trapping tests and ESR detection showed that $\cdot OH$ and $\cdot O_2^-$ were the main active substances for TC degradation in the photo-Fenton system. By further measuring the intermediate products of photodegradation, the degradation pathway of TC-HCl was inferred. The toxicity analysis demonstrated that the overall toxicity of the identified intermediates was reduced in this system. This study provides a theoretical and practical basis for the removal of TC in aquatic environments.

1. Introduction

Antibiotics are a type of drug that can effectively resist bacterial infections and are widely used in industries such as pharmaceuticals and livestock and poultry farming. Some of them, nevertheless, have not yet entirely assimilated and have infiltrated the aquatic environment. They have developed into one of nature's most deadly new water pollutants as a result.[1–3] Due to its strong hydrophilicity and low volatility, tetracycline hydrochloride (TC-HCl), which is ranked second in the world in terms of manufacturing, exhibits excellent persistence in aqueous environments.[4–6] If organisms cannot completely absorb antibiotics taken orally, the majority of them will be expelled from the body as metabolites or in their original form. Antibiotics will eventually infiltrate groundwater through leaching and infiltration after being used as organic fertilizer on agricultural land. Antibiotics, which are biodegradable compounds with high biological activity, persistence, and bio-enrichment, have been identified as a novel contaminant in water environmental media. Antibiotic residues in water are present in trace amounts, but they will eventually build up and move up the food chain, harming the ecosystem and endangering human health. These effects include bacterial resistance growth, disruption of animal and plant growth and reproduction, chronic poisoning of the human body, and the "three causes" effect. China has emerged as the world's most substantial manufacturer and importer of antibiotics.[7–9] As a result, one of the key issues that has to be resolved immediately in the field of environmental protection is the investigation of low-cost and effective advanced antibiotic residue treatment.

Currently, TC-HCl is predominantly destroyed by physical, chemical, and biological mechanisms.[10] However, physical and biological techniques of material degradation are inadequate and contribute to additional contamination. Photocatalytic degradation methodology based on semiconductors has been demonstrated to be one of the chemical techniques used to breakdown pollutants due to its low cost and environmentally beneficial character.[11–15] The hydroxyl radical ($\cdot OH$) produced by the Fenton oxidation process has the benefit that it is not selective and can destroy the majority of organic contaminants in the environment. It positive aspects from robust interference blocking capabilities, a wide application window, mild reaction conditions, and simple operation. H_2O and CO_2 are the ultimate

---

Changchun Univ. Sci. & Technol., Sch Chem. & Environm. Engn., Changchun 130022, P. R. China. E-mail: baosiqi@cust.edu.cn

† Electronic supplementary information (ESI) available. See DOI: https://doi.org/10.1039/d3ra05475f

‡ Co-first authors.

products of the Fenton oxidation process, which satisfies the environmental protection standards of "zero discharge" of wastewater.[7,8] The heterogeneous Fenton, or Fenton-like technology, in particular, not only keeps the benefits of high activity and good stability. It also addresses the classic homogenous Fenton's technological problem bottleneck. The reaction between a photogenerated carrier, water, and oxygen molecules in the system provides the basis for heterogeneous Fenton's process, which results in the production of free radical active species with potent oxidizing properties.[16] As a result, the absorbance of a material has a significant impact on the effectiveness of photocatalytic degradation. Tetracycline degradation of semiconductors with broad band gaps, such as ZnO, TiO_2, and SnO_2, has been extensively researched up to this point.[17–19] However, the poor light consumption rate severely impedes their progress toward practical application, so it is crucial to figure out how to create unique, narrow band gap semiconductors that can effectively utilize the visible light region for TC-HCl degradation.

Layered double hydroxides (LDHs), described by the general formula $[M_{1-x}^{2+}M_x^{3+}(OH)_2]^{x+}$ $[A_{x/n}^{n-}\cdot yH_2O]^{x-}$, where M^{2+}, M^{3+} signify divalent and trivalent metal ions, respectively. The value of x is equal to the molar ratio of $M^{3+}/(M^{2+} + M^{3+})$, and A^{n-} is an n-valent interlayer anion, have widely applied in area such as hydrogen evolution, fire retardants, water cracking and effluent remediation due to their unique layered structure and chemical properties.[20–22] LDHs are a potential class of 3D materials because they have a large specific surface area with enough active sites for adsorbing pollutants as well as the ability to readily control the types of interlaminar ions and surface functional groups. Furthermore, by altering the interlayer ions of LDHs, it is possible to achieve the absorbability of the visible light region. For example, Feng *et al.* have prepared mesoporous NiFe-LDHs photocatalyst *via* a facile hydrothermal route and the results showed that NiFe-LDHs the as-prepared LDHs materials performed superior photocatalytic efficiency to eliminate TC from aqueous water solution.[23] Yu *et al.* have synthesized MoS_2/NiFe–Ni foam by simple electrodeposition and hydrothermal methods, which have a high degradation efficiency of dissolved TC by up to 92% during 100 min reaction time under visible light irradiation.[24] A superior contender for a photocatalyst among the numerous LDHs is 3D NiFe-LDHs, which not only have high visible light absorption capabilities but also have better selective adsorption of pollutants than other LDHs.[25,26] There are, however, few publications on the photocatalytic degradation of tetracycline by NiFe-LDHs, and it is necessary to further investigate and optimize the impact of environmental factors on degradation performance.

The development of 3D NiFe-LDHs nanoflowers was accomplished in the present investigation using a straightforward solvothermal method. The microscopic features such as morphology, crystal composition, types of surface functional groups and absorbance were investigated by SEM, XRD, XPS, FT-IR and UV-vis. Degradation measurements revealed that 3D NiFe-LDHs as synthesized have outstanding TC-HCl elimination efficiency in the photo-Fenton method. In-depth research was also done on the effects of photocatalyst concentration, reaction time, pH level, H_2O_2, common anions, and humic acids on photocatalytic degradation. It was investigated to determine how various antibiotic varieties and differences in water quality impacted the performance of the NiFe-LDHs in real-world applications. Finally, a free radical capture experiment, an electron spin resonance test, and the identification of intermediate products were performed to better understand the mechanism and pathway of TC degradation. This work promoted the transition from theory to practice by laying the theoretical groundwork for the improvement of 3D NiFe-LDHs photocatalytic degradation efficiency.

2. Materials and methods

2.1 Materials

$Ni(NO_3)_2\cdot 6H_2O$, $Fe(NO_3)_3\cdot 9H_2O$, NH_4F, urea, and anhydrous methanol (≥99.5%) were of analytical grade and purchased from Shanghai Macklin Biochemical Co., Ltd. The tetracycline hydrochloride (TC-HCl), oxytetracycline (OTC) and nitrofurantoin (FT) were analytical reagents and purchased from Sinopharm Chemical Reagent Co., Ltd (the molecular information of TC, OTC and FT is shown in Table S1†). All reagents were used as received without further purification.

2.2 Preparation and characterization of NiFe-LDHs

According to previously published literature.[27] NiFe-LDHs was created using a hydrothermal process. In a typical synthesis, a clear salt solution with a Ni^{2+}/Fe^{3+} molar ratio of 2.0 was created by dissolving $Ni(NO_3)_2\cdot 6H_2O$ (5.816 g) and $Fe(NO_3)_3\cdot 9H_2O$ (4.04 g) in methanol anhydrous (30 mL). The salt solution was immediately mixed with urea (1.261 g) and NH_4F (0.1 g) and rapidly agitated for 2 hours. The solution was then placed to a 50 mL stainless steel autoclave that was lined with Teflon. For 12 hours, the autoclave was sealed and kept at 120 °C. By using a centrifugal technique, solid sediment was collected and subjected to three separate washes with distilled water and ethanol. Finally, drying in a vacuum oven produces brown powder particles. Characterization of NiFe-LDHs was provided in the ESI.†

2.3 Catalytic degradation experiment

A 500 W xenon lamp from Anhongda Optoelectronics Technology Co., Ltd in China was used in a photoreaction apparatus that the researchers built themselves to conduct the photocatalytic degradation studies. The sample was 10 cm away from the xenon lamp, and 5000 Lex of light was being emitted. The following experiments were carried out: TC solution (50 mL) was mixed with magnetic stirrers to distribute 30 mg of NiFe-LDHs, and the required amount of H_2O_2 was then added. The mixture was agitated in the dark for 30 minutes prior to illumination to achieve adsorption equilibrium. The xenon lamp used to simulate sunshine was then held over the suspension. At predetermined intervals, a specific volume of analytical sample was quickly removed from the reaction solution and filtered through a 0.22 μm membrane. The maximum absorption band (356 nm) on a UV-vis spectrophotometer (Shanghai

Yuefeng Instrument Co., Ltd, China) was used to determine the concentration of TC, and Lambert–Beer's law was used to determine the residue concentration of the TC solution. The following equation was used to compute the photocatalytic degradation efficiency (μ):

$$\mu = (C_0 - C_t)/C_0 \times 100\% \quad (1)$$

where C_0 is the initial concentration of TC, and C_t is the TC concentration at the corresponding reaction time.

Other water quality investigations and other antibiotic experiments were conducted to evaluate the NiFe-LDHs' practical applicability. The initial photocatalytic reaction's settings were followed for the recycle testing. The synthesis and function of active species in the photo-Fenton process were investigated using quenching experiments and ESR tests, and the intermediate products of photodegradation were identified using UPLC/MS. The decomposition experiment of H_2O_2 was also carried out. After the experiment was completed, the solution was filtered out with filter paper, and the remaining catalyst was dried at 80 °C in the oven and kept at low temperature for recycling.

3. Results and discussion

3.1 Characterization of NiFe-LDHs

SEM measurements were employed to explore the morphology and crystal phase of NiFe-LDHs. As can be seen from Fig. 1a, the synthesized catalyst exhibits an abundant 3D sheet-like network structure, which is a flower-like microporous structure formed by the stacking of smooth thin nanosheets. In addition, the nanosheets are homogeneous in size and measure a thickness of about 30 nm. As described in literature, the observed highly connected sheet-like network may provide broad transportation paths for electron transfer.[28] Furthermore, this three-dimensional structure, which resembles a flower, increases the number of reaction sites and makes adsorption reactions easier. Additionally, the catalyst's surface and interior offer various opportunities for the incident light to reflect and scatter, which enhances the use of visible light. The EDS element mapping maps corresponding to Ni, Fe, C and O in NiFe-LDHs are shown in Fig. 1 respectively. The contents of Ni, Fe, C and O are evenly distributed in the catalyst.

In order to obtain the crystal structure of NiFe-LDHs, X-ray diffraction spectroscopy tests was conducted (Fig. 1b). There were obvious characteristic diffraction peaks at $2\theta = 11.5°$, 23.3°, 34.6°, 39.0°, 46.4°, 60.3°, 61.3° and 65.2°. It is consistent with (003), (006), (012), (015), (018), (110), (113) and (116) on the standard card of hexagonal system NiFe-LDHs (JCPDS 40-0215).[29] And there were no other obvious peaks in the spectrogram, indicating that the purity of the prepared NiFe-LDHs is high.

FT-IR test further analyzed the surface chemical properties, the existence of functional groups, element composition and surface chemical bond of NiFe LDHs. As shown in Fig. 1c, a wide absorption peak was displayed at 3357 cm^{-1}, which could be attributed to the O–H stretching mode of water molecules, with corresponding H–OH vibrations occurring at approximately 1622 cm^{-1}. The strong peak at 1375 cm^{-1} corresponds to NO_3^-, which conforms to the typical characteristics of LDHs.[35–37]

Fig. 1d shows BET and aperture distribution images of NiFe-LDHs. The curve is very similar to that of type IV. According to IUPAC classification, it belongs to H3 hysteresis loops, which is typical mesoporous material.[38] The results of N_2 adsorption show that NiFe-LDHs had a very high specific surface area (216.27 $m^2\ g^{-1}$), and the pore size is mainly concentrated around 1.81 nm. The larger the specific surface area of the catalyst, the larger the contact area with organic pollutants, and then the more active sites involved in adsorption and photocatalytic reactions. Thus it can be seen that NiFe-LDHs is expected to achieve efficient degradation of pollutants.

XPS analysis was conducted to further investigate the composition and surface state of NiFe-LDHs. The wide scan survey spectra (Fig. 2a) verified the co-existence of Ni, Fe, C and O element. As shown in Fig. 2b, O element can be divided into two peaks by Gaussian fitting located at 531.9 eV and 533.5 eV, which corresponded to the lattice oxygen and surface chemisorbed oxygen, respectively.[30] In C 1s spectra (Fig. 2c), the peaks at 284.5 eV, 286.1 eV and 288.4 eV could be assigned to C–C/C=C, C–O and C=O, respectively. The spectrum of Fe 2p (Fig. 2d), exhibited three fitted peaks at 711.49, 714.3, 725.98 eV and 733.9 eV, which corresponded to Fe(II), Fe(III), Fe(II) and Fe(III), respectively.[31–33] Fig. 2e displayed that the fitting peaks of Ni $2p_{3/2}$ and Ni $2p_{1/2}$ were located at 855.4 eV and 873.3 eV, respectively, including two satellite peaks at 879.8 eV and 862.1 eV.[32–34] What is more, because the presence of carbon, two satellite peaks around the main reflection appear at 880.4 eV and 862.1 eV.

The electrochemical test of NiFe-LDHs is depicted in Fig. S1.† The UV-vis DRS test is a significant tool for characterizing light absorption performance since it allows you to see the range and intensity of the catalyst's light response. The estimated band gap of NiFe-LDHs is 2.08 eV, as shown in Fig. S1(a),† and a narrower band gap is favourable to boosting the migration efficiency of photogenerated electrons, hence promoting the degradation of tetracycline hydrochloride. Fig. S1(b)† shows that photoluminescence spectra were acquired at the excitation wavelength of 500 nm using a PL emission spectrum test to investigate the separation and transfer efficiency of the material's photogenerated electron hole pairs. The sample's linear scanning voltammetric curve (LSV) is shown in Fig. S1(c).† The figure shows that NiFe-LDHs has the largest current density at the same point position, indicating the quickest electron transfer rate. Fig. S1(d)† depicts the material's electrochemical impedance spectrum, which reveals that the synthesized NiFe-LDHs have a lower arc radius in the high frequency area than pure $Ni(NO_3)_2$ and $Fe(NO_3)_3$. According to the results of the foregoing electrochemical experiments, the synthesized NiFe-LDHs has a better electron transfer and separation efficiency, which is advantageous for the photocatalytic process.

3.2 TC degradation in the photo-Fenton process

3.2.1 Determination of optimum conditions. To investigate the effect of various NiFe-LDHs doses on the photo-Fenton

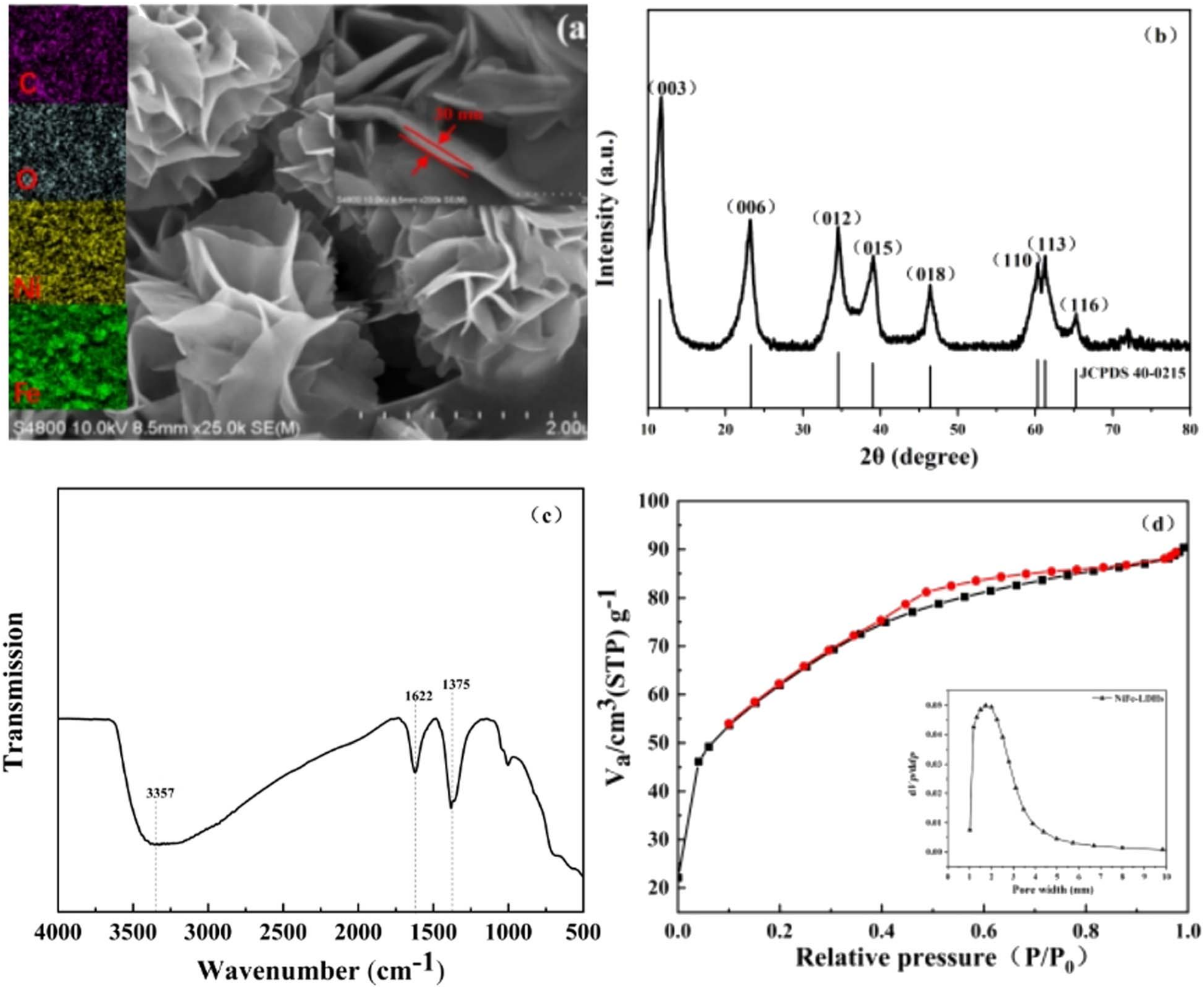

Fig. 1 Structural characterizations of NiFe-LDHs. (a) SEM image, (b) XRD pattern, (c) FT-IR and (d) BET and aperture distribution.

degradation of TC-HCl, five different dosages of NiFe-LDHs were chosen. The degradation rate of TC increased from 3.95% to 63.69% when the dosage of NiFe-LDHs increased from 0 to 30 mg (Fig. 3a). However, the degradation rate of TC dropped from 63.69% to 53.74% as the catalyst dosage continued to increase to 50 mg. This is due to the fact that as the dosage of catalyst increased, the quantity of free radicals and holes generated also grew. Additionally, the contact sites between the catalyst and TC increased, which would promote degradation. However, as the amount of catalyst further increased, excessive catalyst could lead to aggregation, reduced the light transmission through the solution, hindered the production of active substances, and thus inhibited the degradation of TC.[39]

The results of the effects of various initial TC concentrations are displayed in Fig. 3b. The degradation rate increased from 69.47% to 88.69% when the starting concentration of TC increased from 10 mg L^{-1} to 30 mg L^{-1}. The degradation rate decreased from 88.69% to 55.27% as the starting concentration of TC HCl increased to 70 mg L^{-1}. The reason for this phenomenon is that within the low concentration range, as TC concentration increased, the stimulated TC molecules and reactive oxygen species generated by irradiation increased, which boosted photodegradation. However, as TC concentration continued to increase, the color deepening of the solution would impact the transmittance, which was not conducive to the photocatalytic reaction and inhibited the degradation of tetracycline.

The impact of various initial pH levels on the photo-Fenton degradation of TC is depicted in Fig. 3c. In more detail, weak alkalinity facilitated the process, while both acidic and alkaline circumstances prevented it. This is because when the solution weakly alkaline (pH = 8.01), the catalyst was relatively stable, which was conducive to promoting the catalytic performance of the photocatalyst. The lower left corner of Fig. 3c depicts the morphological distribution curve of TC in aqueous solutions as a function of pH. TC is also an amphoteric chemical that exists in many forms under various pH settings.[40] The isoelectric point of NiFe-LDHs was calculated to be 6.97 by calculating the pH-zeta curve (Fig. S2†). When the pH was at 2.09 and 4.2 (smaller than the isoelectric point), the surface of NiFe-LDHs was positively charged due to zwitterions protonation, and the

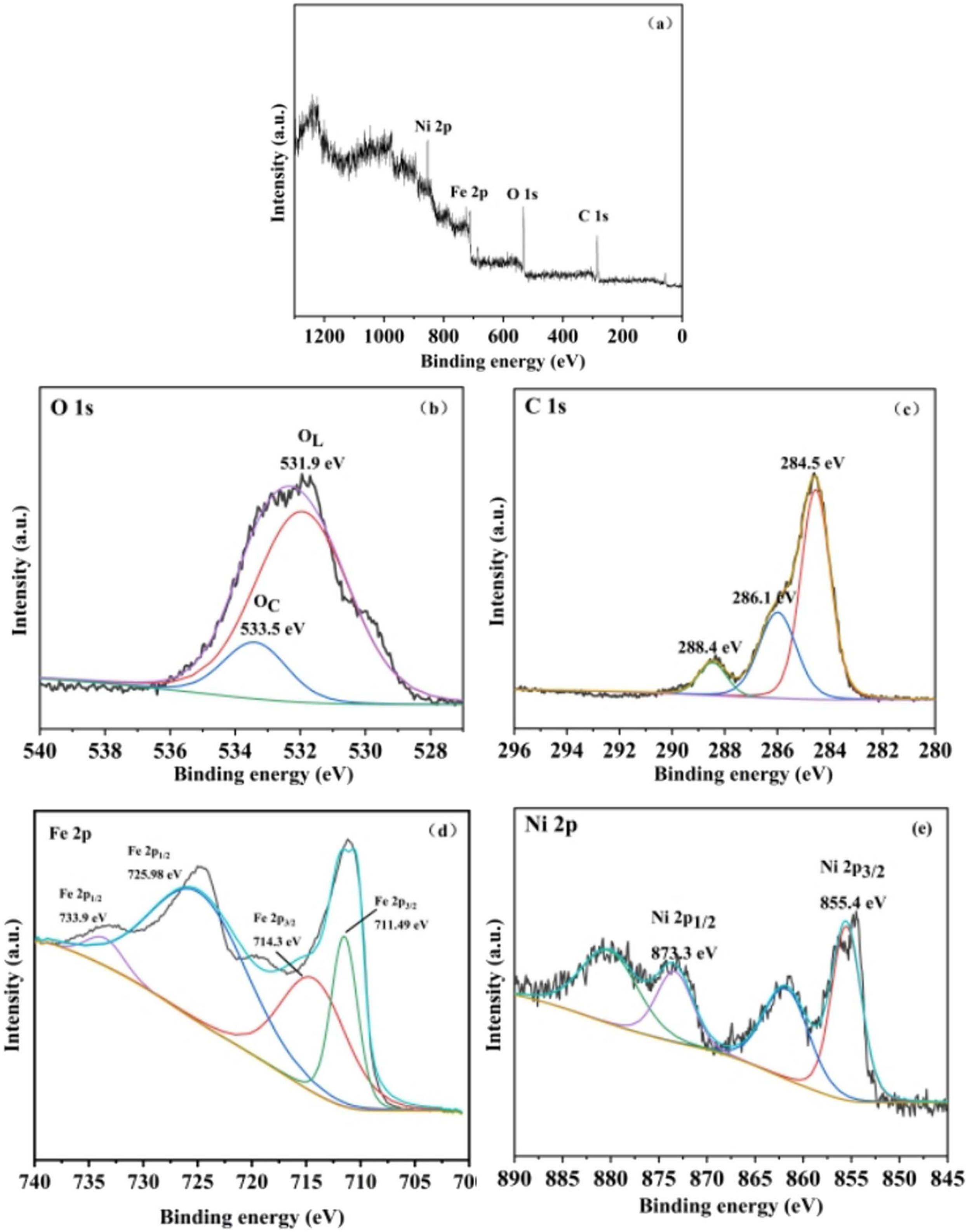

Fig. 2 (a) XPS survey spectra of 3D NiFe-LDHs; (b) XPS O 1s spectrum; (c) XPS C 1s spectrum; (d) XPS Fe 2p spectrum; (e) XPS Ni 2p spectrum.

TC was in a cationic condition. As a result, a electrostatic repulsion was showed, which hindered deterioration. The surface of NiFe-LDHs was negatively charged when the pH was 10.04 (higher than the isoelectric point). TC was in an anionic form (TCH^-) at this stage, and NiFe-LDHs and TC were mutually exclusive. Furthermore, under alkaline conditions, the

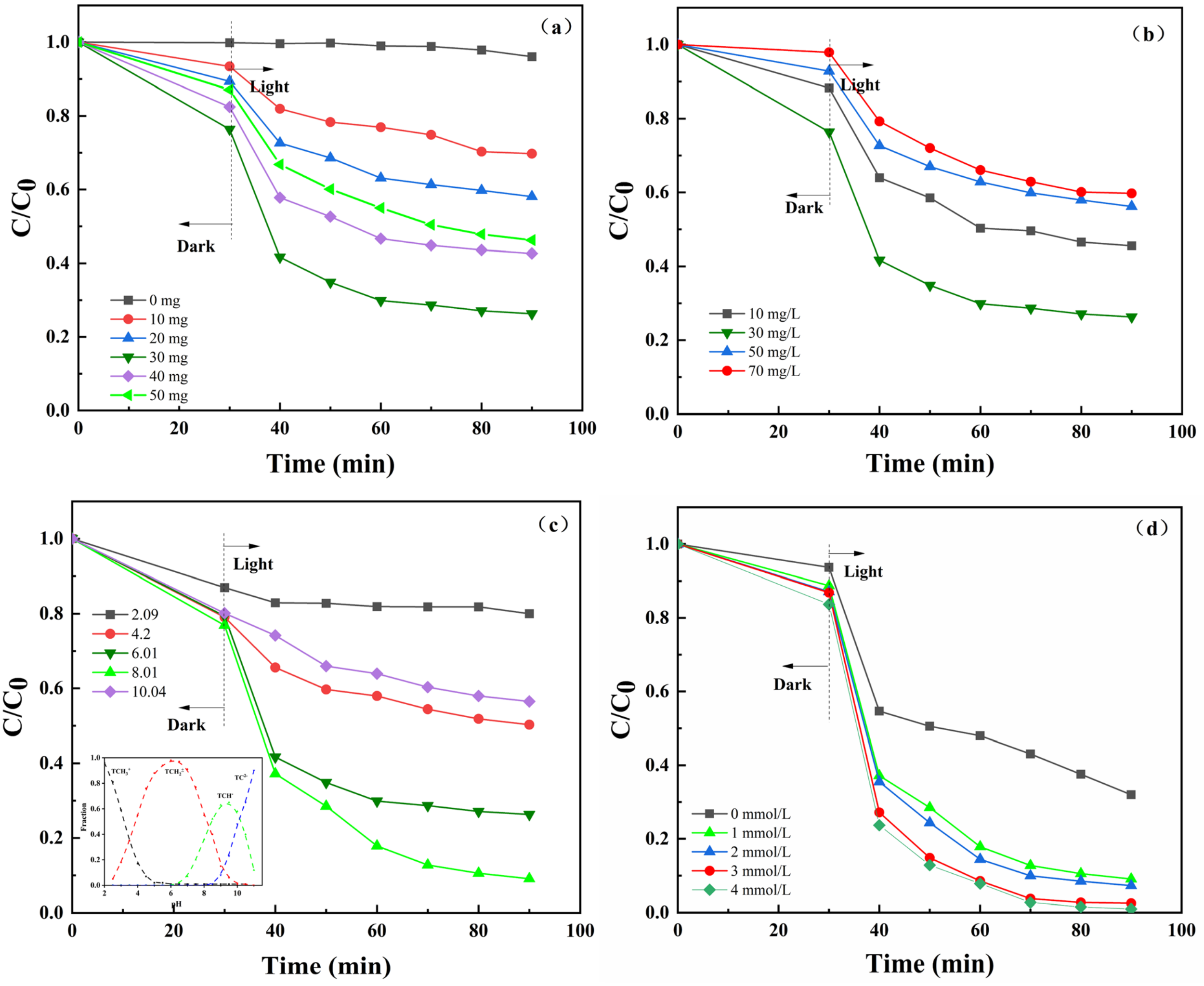

Fig. 3 (a) Effect of NiFe-LDHs dosage on TC degradation in the photo-Fenton process. [TC] = 30 mg L^{-1}, pH = 6.01 and H_2O_2 = 1 mmol L^{-1}, (b) effect of effect of TC concentrations on TC degradation in the photo-Fenton process. NiFe-LDHs dosage = 30 mg, pH = 6.01 and H_2O_2 = 1 mmol L^{-1}, (c) effect of pH on TC degradation in the photo-Fenton process. NiFe-LDHs dosage = 30 mg, [TC] = 30 mg L^{-1} and H_2O_2 = 1 mmol L^{-1}, (d) effect of H_2O_2 concentrations on TC degradation in the photo-Fenton process. NiFe-LDHs dosage = 30 mg, [TC] = 30 mg L^{-1} and pH = 8.01.

degree of deprotonation of tetracycline increases, resulting in a decrease in its breakdown rate.[41,42]

The influence of varying H_2O_2 concentrations on photo-Fenton degradation of TC is shown in Fig. 3d. By raising the H_2O_2 concentration from 1 mmol L^{-1} to 3 mmol L^{-1}, the degradation rate rose from 68.01% to 99.11%. However, when the H_2O_2 concentration was increased to 4 mmol L^{-1}, the degradation rate did not alter considerably. This is due to the fact that under transition metal conditions, H_2O_2 can form hydroxyl radicals (·OH), which promote the decomposition of pollutants. As the concentration of H_2O_2 increased, ·OH generation increased. However, as the concentration of H_2O_2 continued to increase, excess H_2O_2 in the system depleted ·OH in the system, causing the reaction rate no longer increased. The findings are consistent with prior findings.[43] Therefore, from the perspective of environmental protection, 3 mmol L^{-1} is selected as the optimal concentration of H_2O_2 to continue the follow-up experiment.

3.2.2 Degradation performance of TC under the optimum conditions. Batch studies were carried out to investigate the degradation of TC in various settings, and the findings are given in Fig. 4a. It is obvious from Fig. 4a that TC did not degrade fundamentally under visible light, showing that TC was resistant to visible light. The degradation of TC was marginally accelerated with the addition of H_2O_2 to the solution, which probably because H_2O_2 created ·OH under light circumstances, encouraging the breakdown of TC. When Ni^{2+} + Fe^{3+} and H_2O_2 are added to the system under light conditions, approximately 71% of the tetracycline is eliminated; however, Ni^{2+} and Fe^{3+} added to the homogeneous system will all dissolve in the reaction solution and are difficult to recover after the reaction, requiring additional experimental expenses. In the NiFe LDHs/vis system, the degradation rate of TC reached 68.01% due to the photocatalytic effect. With the addition of H_2O_2 to the solution, the rate of TC degradation was further accelerated and eventually reached 99.11%, which is a typical heterogeneous

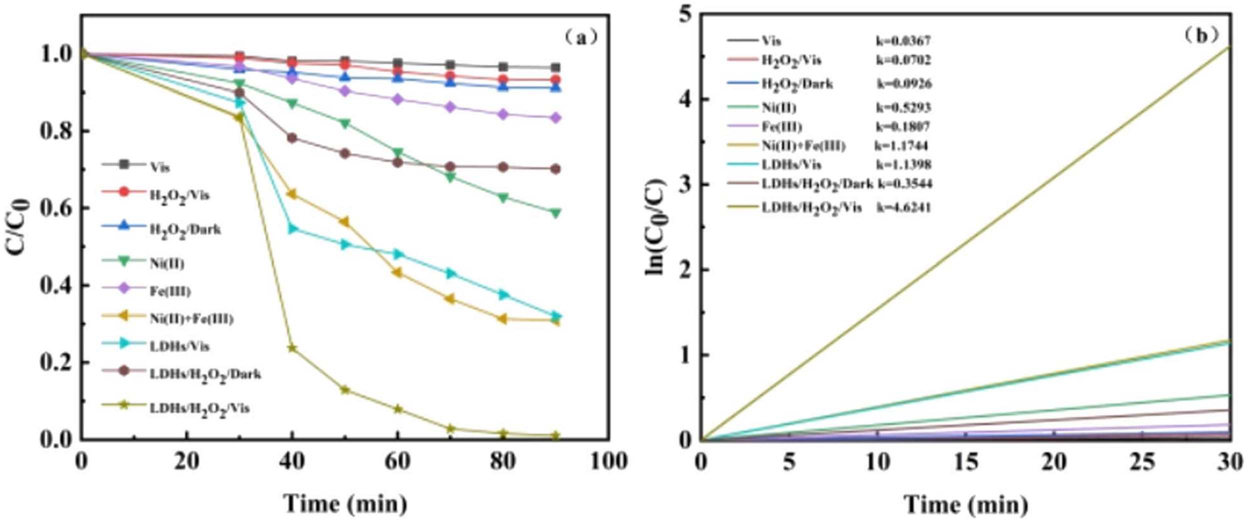

Fig. 4 (a) Degradation of TC in different systems, (b) reaction kinetics fitting curves.

photo-Fenton process. The apparent rate constant of TC degradation was estimated by fitting pseudo first order, and the results are shown in Fig. 4b. The outcomes demonstrated that all reactions adhered to the first-order kinetic equations. The first-order kinetic constant of TC in the photo-Fenton system is 4.09 times than that of the NiFe-LDHs/vis system, indicating that H_2O_2 played a significant role in the formation of active species. Additionally, the *k* of the NiFe-LDHs/H_2O_2/vis system is 13.2 times than that of the NiFe-LDHs/H_2O_2 system, demonstrating that visible light can encourage the formation of charge carriers, thereby promoting degradation. The characteristics of NiFe-LDHs are compared to those of other photocatalytic materials in Table 1. It is apparent from the analyses done that this effort has produced a suitable photocatalyst.

3.2.3 Effect of environmental factors on TC degradation.

Since multiple ions and humic acid are ubiquitous in the water environment, the influence of four typical inorganic ions (Cl^-, CO_3^{2-}, Fe^{2+} and Ca^{2+}) and humic acid (HA) on TC degradation in LDHs/H_2O_2/vis system was studied.[53] It is obviously observed that the degradation of TC was inhibited after the addition of Cl^- and CO_3^{2-}. The reason is that Cl^- and CO_3^{2-} consume ·OH in the system as scavengers of ·OH (eqn (2)–(5)).[53,54] On the contrary, the presence of Fe^{2+} and Ca^{2+} promoted the degradation of TC. The facilitation of Fe^{2+} because it reacts with dissolved oxygen in the system to generate superoxide anion radicals (·O_2^-) and Fe^{3+} (eqn (6) and (7)), and Fe^{3+} can further generate ·OH under visible light, promoting degradation. Ca^{2+} exhibited an enhancing effect because Ca^{2+} could recombine

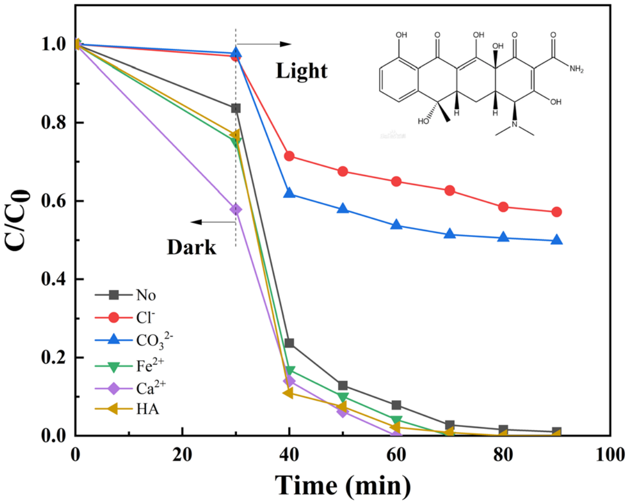

Fig. 5 Effect of anions, cations and HA on TC degradation in the photo-Fenton process.

Table 1 Comparison of the present research with similar studies done before

Material	Light source	Working solution	Degradation rate	pH	Ref.
P–CdS@NiFe-LDH	300 W Xe lamp	30 mg photocatalyst 30 mL MO (10 mg L^{-1})	98% (100 min)	—	44
$FeCoZnO_4$/CuCr-LDH	Vis-light($\lambda \geq 400$ nm)	0.5 g L^{-1} catalyst 50 μM caffeine	66.5% (120 min)	8	45
Fe_2O_3/Zn–Al-LDH	UV-vis-light	0.01 g catalyst 100 mL OII (40 mg L^{-1})	81.2% (5 h)	6.7	46
Cu–Zn–Fe-LDH	UV-vis-light	0.5 g L^{-1} catalyst 250 mL PR and arsenic (1 mg L^{-1})	99% (10 h)	7	47
FePcS-PMA-LDH	500 W Xe lamp	40 mg catalyst 100 mL BPA (10 mg L^{-1})	100% (100 min)	6	48
ND/CuFe-LDH	500 W Xe lamp	0.0667 g L^{-1} 75 mL MB (10 mg L^{-1})	93.5% (120 min)	—	49
M_3Cr–CO_3-LDH	150 W halogen lamp	0.5 g catalyst 25 mg MB (5 mg L^{-1})	90.67 (140 min)	—	50
(Co–Mg)Al-LDH	UV-vis-light	0.05 g catalyst 500 mL solvent	10% (5 h)	—	51
MnMgFe-LDH	UV-vis-light	30 mg catalyst 100 mL MB (20 ppm)	92% (300 min)	7	52
NiFe-LDH	500 W Xe lamp	30 mg catalyst 50 mL TC (30 mg L^{-1})	99.11 (90 min)	6.01	This work

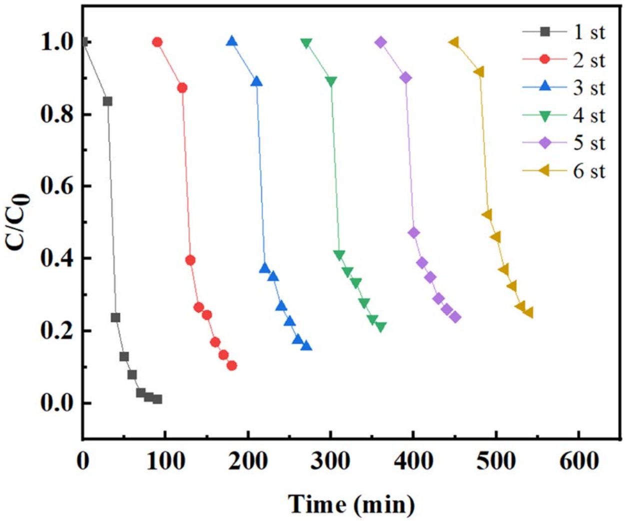

Fig. 6 Recycling experiments of NiFe-LDHs in the photo-Fenton process.

with N4–OH12a on the A ring and the O10–O12 on the BCD ring of TC (upper right corner of Fig. 5), thereby depleting tetracycline hydrochloride TC and promoting degradation.[55,56] Low concentration (5 mg L^{-1}) of HA played a promoting role, and high concentration (20 mg L^{-1}) played an inhibitory role. This is because HA has both photosensitizing and shading effects. Photosensitization is due to that HA generated ·OH, H_2O_2 and $\cdot O_2^-$ through type I (eqn (8)) and $^1O_2$ through type II (eqn(9)), and these active substances generated promoted the degradation of TC.[60] Instead, HA competed with TC for active groups to inhibit degradation. Therefore, the role of HA in the photo-Fenton degradation of TC depends on the balance between the two opposite effects.[57]

$$\cdot OH + Cl^- \rightarrow Cl\cdot + OH^- \tag{2}$$

$$CO_3^{2-} + H^+ \rightarrow HCO_3^- \tag{3}$$

$$HCO_3^- + \cdot OH \rightarrow H_2O + CO_3^- \tag{4}$$

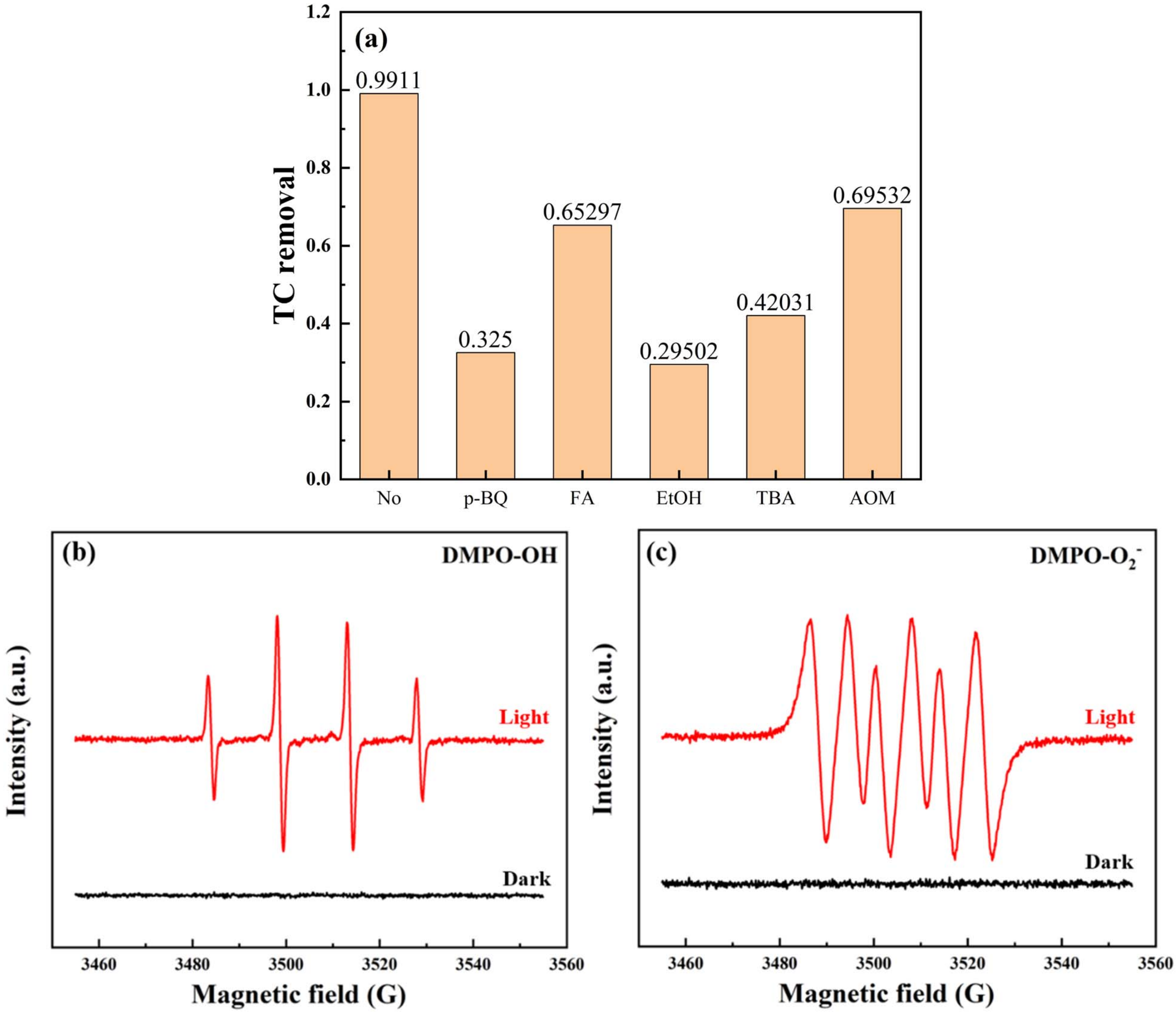

Fig. 7 The effects of different scavengers on TC degradation in the photo-Fenton process and EPR spectra of (b) DMPO-·OH, (c) DMPO-$\cdot O_2^-$.

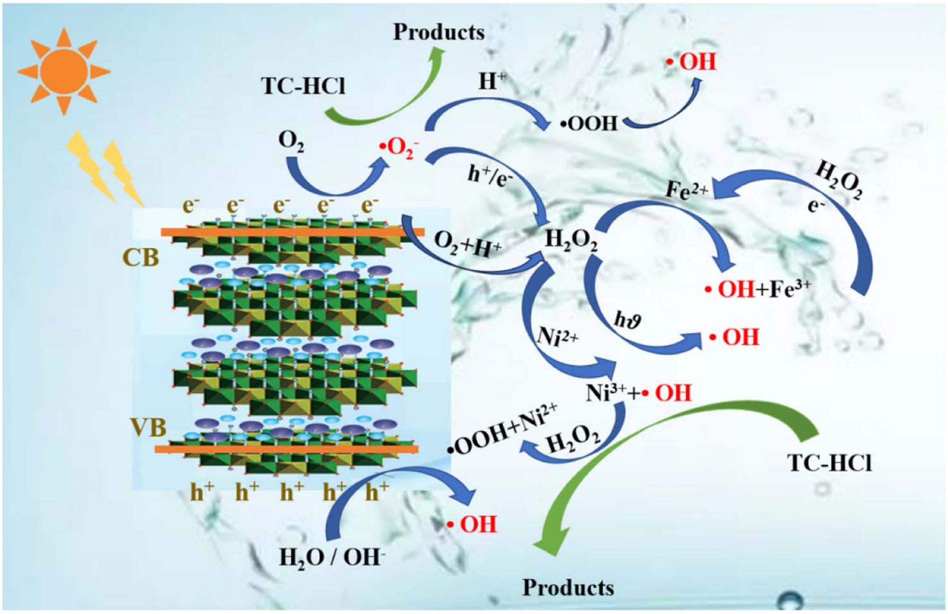

Fig. 8 Proposed mechanisms of the degradation of TC in the photo-Fenton process.

$$\mathrm{CO_3}^{2-} + \cdot\mathrm{OH} \rightarrow \mathrm{OH}^- + \mathrm{CO_3}^- \tag{5}$$

$$\mathrm{Fe}^{2+} + hv \rightarrow \mathrm{Fe}^{3+} + \mathrm{e}^- \tag{6}$$

$$\mathrm{O_2} + \mathrm{Fe}^{2+} \rightarrow \mathrm{Fe}^{3+} + \cdot\mathrm{O_2}^- \tag{7}$$

$$\mathrm{HA} \xrightarrow{hv} 1\mathrm{HA}^* \rightarrow {}^3\mathrm{HA}^* \rightarrow \cdot\mathrm{OH}/\mathrm{H_2H_2}/\cdot\mathrm{O_2}^- \tag{8}$$

$$\mathrm{HA} \xrightarrow{hv} 1\mathrm{HA}^* \rightarrow {}^3\mathrm{HA}^* \xrightarrow{\mathrm{O_2}} 1\mathrm{O_2} \tag{9}$$

3.2.4 Environmental compatibility. Four different water quality were chosen: tap water, pure water (Wahaha water), automobile factory wastewater (the water quality is provided in Table S2†), and domestic sewage, and the degradation rates were 83.66%, 83.66%, 74.04%, and 74.04%, respectively (Fig. S3(a)†). Under different water quality conditions, the removal of TC showed relatively ideal results. However, due to the complexity of its components, domestic sewage and automobile factory wastewater exhibited a significant inhibitory effect on the decomposition of TC compared to distilled water. Hence one can see that NiFe LDHs can effectively decompose TC contaminants in various water qualities. Furthermore, two other antibiotic pollutants, OTC and FT were selected to study. It can be seen from Fig. S3(b)† that NiFe-LDHs has a good degradation effect not only on TC, but also on OTC and FT, which verifies the broad spectrum of NiFe-LDHs and has the potential to degrade more antibiotic pollutants.

To investigate the stability of NiFe-LDHs, six cycle experiments were performed. NiFe-LDHs showed good stability after repeated degradation of TC for six times (Fig. 6). At the end of the sixth cycle experiment, the degradation rate of TC was 75.99%, which was lower than that of the first photocatalytic experiment (99.11%). This may be related to the dissolution of metal ions, the adsorption of reaction intermediates and the loss of catalysts during centrifugation.[58] Moreover, during the cycle experiment, the adsorption performance of the catalyst continue to decrease, which also affect the degradation rate of TC. However, the performance of the catalyst did not degrade much after the six cycles of the experiment, and the degradation performance remained stable after that. Fig. S4† shows the XPS spectra of NiFe-LDHs after 6 cycles. We can see that Ni, Fe, C and O elements in the XPS spectra before and after the reaction do not change, but the peak height and peak area change slightly, indicating that REDOX reactions occur on the surface of the material. At the same time, the content changes of nickel and iron ions before and after the reaction were calculated, as shown in Table S4.† It can be found from the table that for nickel ion, the percentage of Ni^{2+} and Ni^{3+} before the reaction is 24.0% and 75.1% respectively, while the percentage of Ni^{2+} and Ni^{3+} after the reaction is 37.85% and 62.15% respectively, indicating that 12.95% of Ni^{3+} is converted into Ni^{2+}. Similarly, for iron ion, 18.11% of Fe^{2+} was converted to Fe^{3+}. The ionic leaching amounts of Ni^{2+} and Fe^{3+} were further determined. After 6 cycles of experiments, the ion leaching amounts of Ni^{2+} and Fe^{3+} decreased to 3.92 mg L^{-1} and 3.14 mg L^{-1}, respectively, and the ion leaching amounts were still reduced. However, both leaching amounts are slightly higher than international standards. There are two primary causes of metal ion leaching: (1) during the reaction process, the valence state of metal REDOX decreases, resulting in a change in the chemical characteristics of the corresponding metal elements, resulting in metal ion leaching;[59] (2) because the sample is shipped to other institutes for analysis, the extended soaking time causes solution evaporation and corrosion of the metal material, resulting in an increase in the metal leaching amount that is greater than the real metal leaching amount.

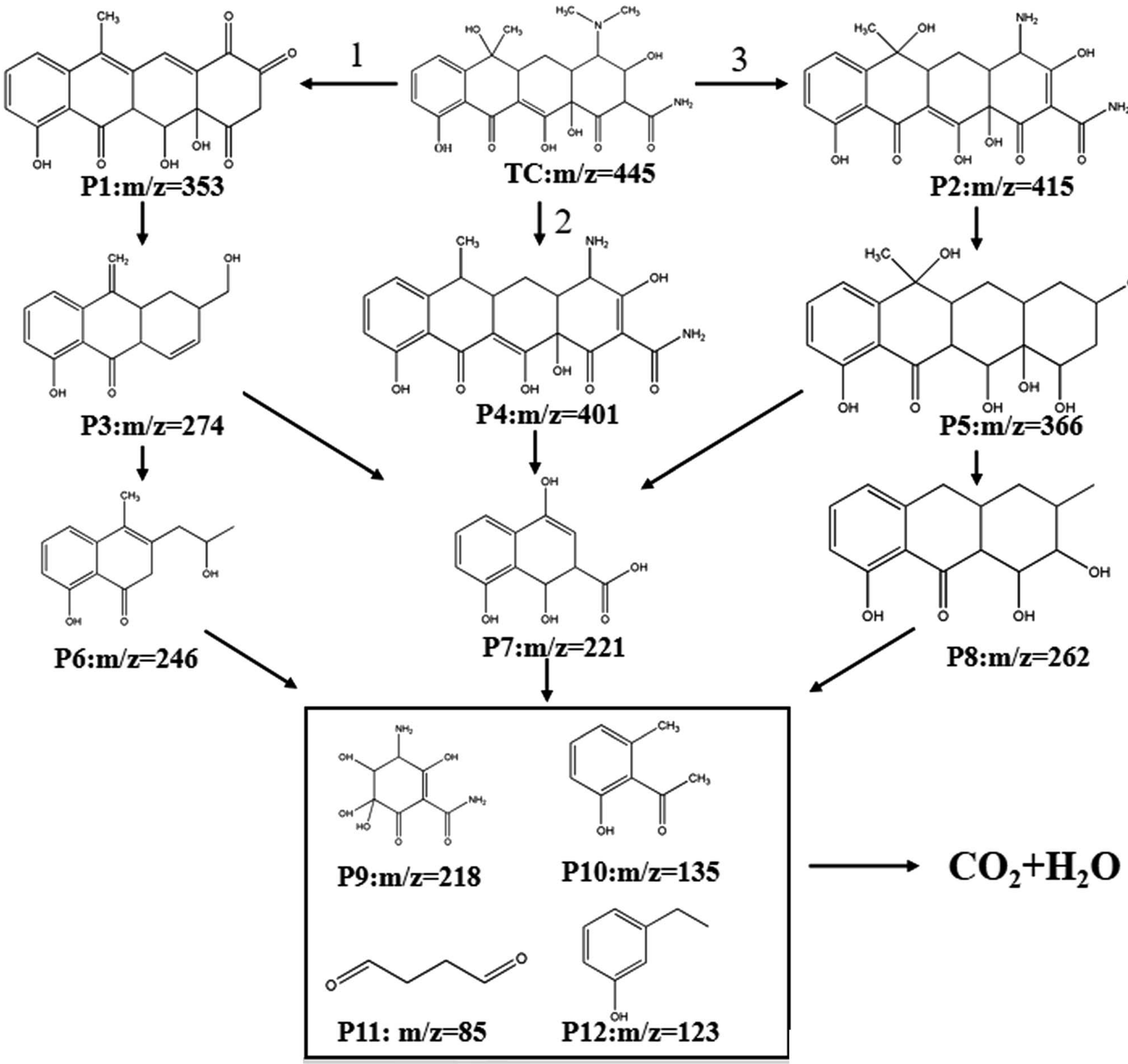

Fig. 9 Potential degradation pathways of TC in the photo-Fenton process.

In future trials, we plan to mix NiFe-LDHs with additional materials to further limit metal leaching.[60] In future trials, we intend to further reduce the amount of ion leaching by mixing it with other materials, with the goal of meeting national standards. To properly comprehend the stability feature, SEM and XRD characterizations of fresh and after 6 runs NiFe-LDHs were examined. As can be seen in Fig. S5(a),† although the characteristic diffraction peak overall diminished, the XRD patterns showed that the crystal structure of NiFe-LDHs was still intact. This may be because the crystal form deteriorated during continuous run. In addition, after six cycles, the morphology of three-dimensional nano-flowers changed, as shown in Fig. S5(b),† which may be caused by structural collapse during the reaction process. Overall, NiFe-LDHs has good stability, recyclability and prospects in practical applications.

3.3 The possible mechanism of TC degradation

The quenching experiments of active substance (ROS) were carried out to study the degradation mechanism. Ammonium oxalate (AOM), *p*-benzoquinone (*p*-BQ), furfuryl alcohol (FA), ethanol (EtOH) and *tert*-butanol (TBA) are added to the system as quenchers for h^+, $\cdot O_2^-$, $^1O_2$, catalyst surface $\cdot$OH and solution $\cdot$OH, respectively.[61] It can be seen from Fig. 7a that the addition of five quenchers all had different inhibitory effects on the degradation of TC, among which ethanol and *p*-BQ showed the greatest inhibitory effects, indicating that catalyst surface $\cdot$OH and $\cdot O_2^-$ were the main active substances in the system. Subsequently, ESR tests were performed to observe the magnetic resonance signal of electrons by comparing the dark and visible light conditions, so as to verify the active free radicals that play major roles in the

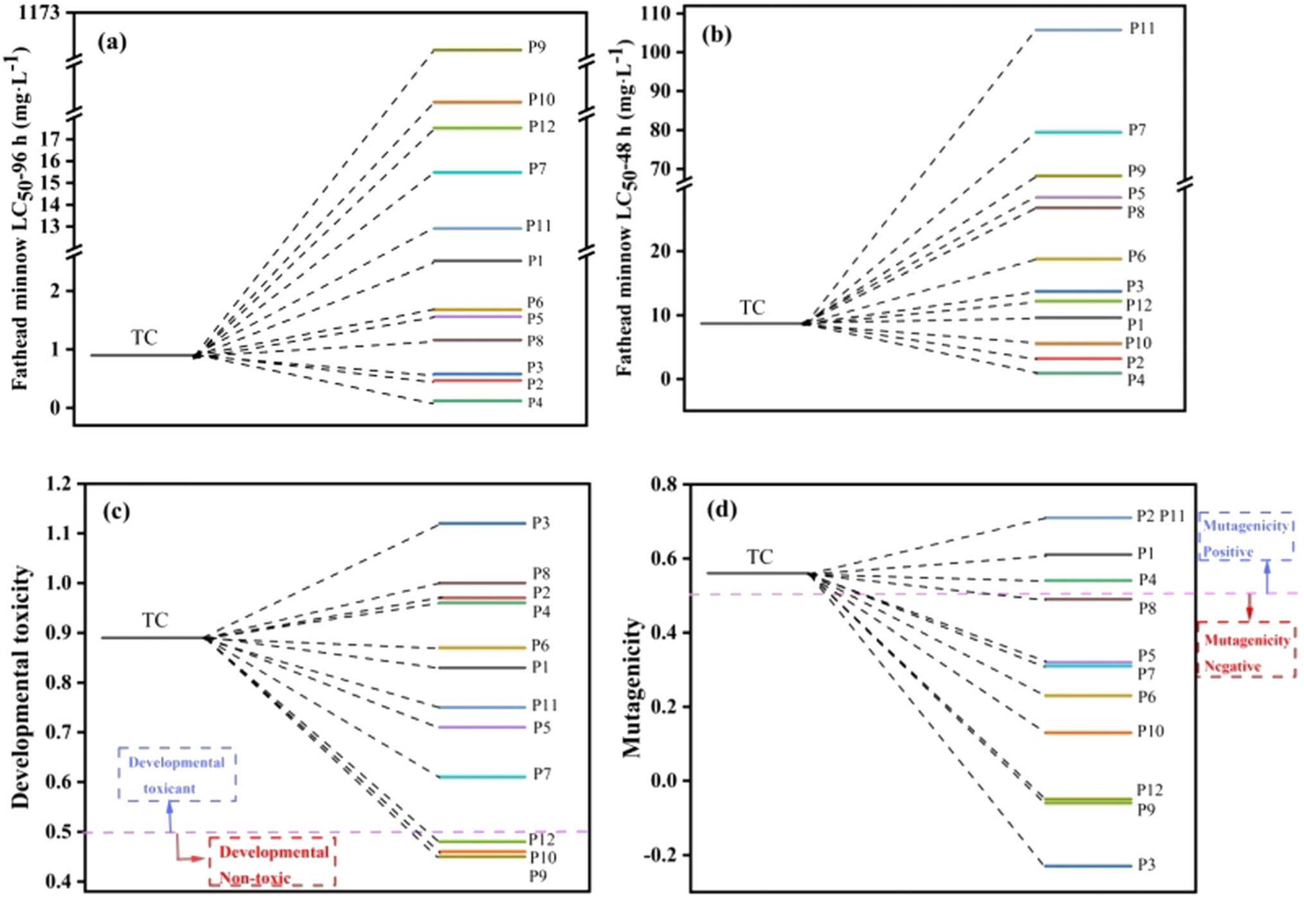

Fig. 10 The fathead minnow LC 50–96 h (a), daphnia magna LC50-48 h (b), developmental toxicity (c) and mutagenicity (d) of tetracycline and its possible degradation intermediates.

system. The ESR signals of DMPO-$\cdot OH$ and DMPO-$\cdot O_2^-$ did not show obvious ESR signals under dark conditions (Fig. 7b and c). On the contrary, both DMPO-$\cdot OH$ and DMPO-$\cdot O_2^-$ showed strong signal peaks under visible light, demonstrating that $\cdot O_2^-$ and $\cdot OH$ are the main active substances, which is consistent with the results of the quenching experiments.[62] Furthermore, the breakdown of H_2O_2 was determined. The decomposition of H_2O_2 was further determined, as shown in Fig. S6.† The experimental results show that the self-decomposition rate of H_2O_2 is 14.35%, indicating that H_2O_2 mainly promotes the formation of active substances through the REDOX reaction with NiFe-LDHs, resulting in the valence transformation of metals, thus promoting the catalytic reaction.

The degradation mechanisms are depicted in Fig. 8. At the initial stage of the reaction, 17.4% of TC was adsorbed onto catalyst surface due to its substantial specific surface area. NiFe-LDHs then produced photo-generated electrons (e^-) and photo-generated holes (h^+) in the presence of visible light (eqn (10)).[63] Subsequently, h^+ reacted with H_2O or OH^- in the system to produce $\cdot OH$ (eqn (11) and (12)). e^- reacted with $\cdot O_2^-$ on the catalyst surface to form $\cdot O_2^-$ (eqn (13)), and then generated $\cdot OH$ with stronger oxidation capacity (eqn (14)–(16)). Additionally, H_2O_2, a potent oxidant, can substantially lower the chances of e^- and h^+ recombination and produce a significant amount of $\cdot OH$ to support photocatalyst activity (eqn (17)).[64] Under visible light, Fe^{3+} can simultaneously produce $\cdot OH$ and Fe^{2+} (eqn (18)), which is necessary for the subsequent heterogeneous Fenton reaction (eqn (19)).[65] Fe (III/II) and Ni (II/III) conversion during the entire reaction phase sped up the reaction (eqn (19)–(23)). In order for TC to entirely degrade into small molecules or even completely mineralize into CO_2 and H_2O (eqn (24)), the produced $\cdot OH$ and $\cdot O_2^-$ attacked the bonds in TC that are difficult to break.

$$\text{3D NiFe-LDHs} + h\nu \rightarrow \text{3D NiFeLDHs}\ (h^+ + e^-) \tag{10}$$

$$h^+ + H_2O \rightarrow H^+ + \cdot OH \tag{11}$$

$$h^+ + OH^- \rightarrow \cdot OH \tag{12}$$

$$O_2 + e^- \rightarrow \cdot O_2^- \tag{13}$$

$$\cdot O_2^- \xrightarrow{H^+} \cdot OOH \xrightarrow{H_2O_2} \cdot OH \tag{14}$$

$$\cdot O_2^- \xrightarrow{h^+} H_2O_2 \xrightarrow{e^-} \cdot OH \tag{15}$$

$$\cdot O_2^- \xrightarrow{e^-} H_2O_2 \xrightarrow{e^-} \cdot OH \quad (16)$$

$$H_2O_2 + \text{visible light} \rightarrow \cdot OH + OH^- \quad (17)$$

$$Fe^{3+} + OH^- + h\nu \rightarrow Fe^{2+} + \cdot OH \quad (18)$$

$$Fe^{2+} + H_2O_2 \rightarrow Fe^{3+} + \cdot OH + OH^- \quad (19)$$

$$Fe^{3+} + H_2O_2 \rightarrow Fe^{2+} + \cdot OOH + 2H^+ \quad (20)$$

$$Ni^{2+} + H_2O_2 \rightarrow Ni^{3+} + \cdot OH + OH^- \quad (21)$$

$$Ni^{3+} + H_2O_2 \rightarrow Ni^{2+} + \cdot OOH + OH^- \quad (22)$$

$$Ni^{3+} + Fe^{2+} \rightarrow Ni^{2+} + Fe^{3+} \quad (23)$$

$$\cdot OH/\cdot O_2^- + TC\text{–}HCl \rightarrow \text{byproducts} + CO_2 + H_2O \quad (24)$$

3.4 The possible degradation pathway of TC and toxicity analysis

Based on the detection of intermediates by UPLC-MS (Table S3†) and previous literature reports.[66–68] three potential degradation pathways were speculated, as shown in Fig. 9. Three potential degradation pathways were suggested, and a total of seven stable intermediate products were found. For process 1, tetracycline undergoes h^+-induced demethylation, oxidation and dehydration reaction, which results in continual ring-opening and eventual decarboxylation, to yield the intermediate (m/z = 246).[69] The tetracycline molecule undergoes demethylation, deamination, and hydroxylation to yield the intermediate (m/z = 221) for process 2. The third method involves first releasing the C=C bond from the tetracycline molecule, followed by the removal of the amide group to produce the related intermediate (m/z = 262). The different intermediates are ultimately totally reduced into the environmentally favorable substances CO_2 and H_2O by further oxidation into smaller molecules (m/z = 218, 165, 146, and 85).

The lethal concentrations of 50% fathead minnow (LC_{50}-96 h) and daphnia magna (LC_{50}-48 h) were evaluated by Toxicity Estimation Software Tool (TEST) based on QSAR to determine the toxicity of TC and intermediates (Fig. 10a and b).[70] The calculations revealed that the lethal concentrations of the intermediates were much lower than those of TC, except for P2, P3, P4 (LC_{50}-96 h) and P2, P4, P10 (LC_{50}-48 h).[71] Fig. 10c demonstrates that the developmental toxicity of intermediates was greatly decreased compared to TC, with the exception of P2, P3, P4, and P8, and P9, P10, and P12 (ref. 72) even becoming "developmental non-toxic." TC, P1, P2, P4, and P11 were positive in terms of mutagenicity (Fig. 10d), whereas the mutagenicity of other intermediates changed from positive to negative. The toxicity prediction stated above states that while some intermediates are still dangerous, they can be totally converted into intermediates that are less toxic by prolonging the reaction period. As a result, the total toxicity of TC was reduced in the photo-Fenton process.

4. Conclusion

By optimizing the reaction conditions, flower-like structured NiFe-LDHs was fabricated in this study using a one-step hydrothermal technique for effective TC elimination in the photo-Fenton process. Under optimal conditions, the NiFe-LDHs/H_2O_2/vis system performed well with very high efficiency, and the degradation rate of TC reached 99.11% within 90 minutes, which is superior to other reported materials. Meanwhile, this high activity of NiFe-LDHs was also suitable for multiple refractory antibiotic, different water quality conditions, and could maintain even in presence of various environmental anions and HA. The heterogeneous catalyst NiFe-LDHs was simple to recover following the reaction, and the amount of nickel and iron ions that leached were relatively low. It can be recycled and maintain excellent catalytic stability and reusability in the subsequent 6 reactions, showing enormous potential in real-world wastewater treatment. The separation of photogenerated carriers and the production of ROS, which aided in the degradation of TC, were encouraged by the Ni(II/III)/Fe(II/III) cycle on the surface of NiFe-LDHs. According to quenching experiments and EPR analysis, photogenerated h^+, $\cdot O_2^-$, $\cdot OH$, and $^1O_2$ all took part in the process and $\cdot OH$ and $\cdot O_2^-$ dominated the breakdown of TC. Through LC-MS recognization of potential intermediates and TEST toxicity analysis, it was found that the degradation of TC by NiFe-LDHs in the photo-Fenton process is a reaction with significantly reduced toxicity. In subsequent experiments, NiFe-LDH needs to be modified to further accelerate the degradation rate of TC and reduce the leaching amount of metal ions.

Conflicts of interest

There are no conflicts to declare.

Acknowledgements

This work was financially supported by Joint Fund Project of the Natural Science Foundation of Jilin Province (YDZJ202101ZYTS076).

References

1 N. Chandel, V. Ahuja and R. Gurav, *Sci. Total Environ.*, 2022, **825**, 153895.
2 W. Zhou, B. Yang and G. Liu, *J. Colloid Interface Sci.*, 2022, **615**, 849–864.
3 Z. Qi, G. Li and M. Wang, *Water Res.*, 2022, **215**, 118240.
4 D. Zheng, G. Yin and M. Liu, *Sci. Total Environ.*, 2021, **777**, 146009.
5 M. Habibi, A. Habibi-Yangjeh and S. R. Pouran, *Colloids Surf., A*, 2022, **642**, 128640.
6 X. Liu, Q. Li and Y. Fan, *Mater. Lett.*, 2022, **315**, 132010.
7 S. Nasseri, A. H. Mahvi and M. Seyedsalehi, *J. Mol. Liq.*, 2017, **241**, 704–714.
8 Y. Wang, L. Wang and Z. Xiao, *J. Alloys Compd.*, 2022, **900**, 163450.

9 D. P. Sahoo, S. Patnaik and K. Parida, *ACS Omega*, 2019, **4**(12), 14721–14741.

10 A. Zaher, M. Taha and R. K. Mahmoud, *J. Mol. Liq.*, 2021, **322**, 114546.

11 A. Tiwari, A. Shukla and D. Tiwari, *J. Ind. Eng. Chem.*, 2019, **69**, 141–152.

12 Y. Liu, J. Tian and L. Wei, *Sep. Purif. Technol.*, 2021, **257**, 117976.

13 N. Farhadian, R. Akbarzadeh and M. Pirsaheb, *Int. J. Biol. Macromol.*, 2019, **132**, 360–373.

14 Y. Li, Z. Lai and Z. Huang, *Appl. Surf. Sci.*, 2021, **550**, 149342.

15 S. Das and Y. H. Ahn, *Chemosphere*, 2022, **291**, 132870.

16 S. Wu, X. Li and Y. Tian, *Chem. Eng. J.*, 2021, **406**, 126747.

17 A. Zyoud, W. Jondi and N. AlDaqqah, *Solid State Sci.*, 2017, **74**, 131–143.

18 Y. Li, Q. Zhang and Y. Lu, *Ceram. Int.*, 2022, **48**(1), 1306–1313.

19 A. O. Oluwole and O. S. Olatunji, *Environ. Sci. Eur.*, 2022, **34**, 1–14.

20 Y. Yu, D. Chen and W. Xu, *J. Hazard. Mater.*, 2021, **416**, 126183.

21 C. Liu, S. Mao and M. Shi, *J. Hazard. Mater.*, 2021, **420**, 126613.

22 J. O. Eniola, R. Kumar and O. A. Mohamed, *J. Saudi Chem. Soc.*, 2020, **24**(1), 139–150.

23 X. Feng, X. Li and H. Luo, *J. Solid State Chem.*, 2022, **307**, 122827.

24 J. Yu, S. Cong and B. Liu, *J. Environ. Chem. Eng.*, 2022, **10**, 108437.

25 H. Wang, Y. Chen and W. Xie, *Int. J. Electrochem. Sci.*, 2019, **14**, 7961–7972.

26 F. Pazoki, S. Bagheri and M. Shamsayei, *Mater. Chem. Phys.*, 2020, **253**, 123327.

27 S. Anantharaj, K. Karthick and M. Venkatesh, *Nano Energy*, 2017, **39**, 30–43.

28 S. He, R. Yin and Y. Chen, *Chem. Eng. J.*, 2021, **423**, 130172.

29 Q. Wang and D. O'Hare, *Chem. Rev.*, 2012, **112**(7), 4124–4155.

30 C. Lei, W. Li and G. Wang, *Chem. Res. Chin. Univ.*, 2021, **37**, 293–297.

31 N. Yang, C. Tang and K. Wang, *Nano Res.*, 2016, **9**, 3346–3354.

32 C. Xiao, Y. Li and X. Lu, *Adv. Funct. Mater.*, 2016, **26**(20), 3515–3523.

33 L. Zhang, R. Zhang and R. Ge, *Chem. – Eur. J.*, 2017, **23**(48), 11499–11503.

34 A. N. Mansour, *Surf. Sci. Spectra*, 1994, **3**(3), 231–238.

35 A. Khataee, T. S. Rad and S. Nikzat, *Chem. Eng. J.*, 2019, **375**, 122102.

36 D. Huang, J. Ma and L. Yu, *Sep. Purif. Technol.*, 2015, **156**, 789–794.

37 K. M. Parida, M. Sahoo and S. Singha, *J. Mol. Catal. A: Chem.*, 2010, **329**(1–2), 7–12.

38 L. Liu, S. Li and Y. An, *Catalysts*, 2019, **9**(2), 118.

39 R. J. Watts and S. E. Dilly, *J. Hazard. Mater.*, 1996, **51**(1–3), 209–224.

40 Z. Li, C. Guo and J. Lyu, *J. Hazard. Mater.*, 2019, **373**, 85–96.

41 T. Soltani, A. Tayyebi and B. K. Lee, *Environ. Manage.*, 2019, **232**, 713–721.

42 L. Chen, D. Ding and C. Liu, *Chem. Eng. J.*, 2018, **334**, 273–284.

43 I. Velo-Gala, J. A. Pirán-Montaño and J. Rivera-Utrilla, *Chem. Eng. J.*, 2017, **323**, 605–617.

44 C. Lai, F. Huang and G. Zeng, *Chemosphere*, 2019, **224**, 910–921.

45 B. Fang, Z. Xing, M. Guo and Y. Qiu, *Sep. Purif. Technol.*, 2021, **274**, 119066.

46 A. Fazli, M. Brigante, A. Khataee and G. Mailhot, *Chemosphere*, 2022, **291**, 132920.

47 Q. Li, G. Wei, Y. Yang, Z. Li, L. Zhang, L. Shao and S. Lai, *Catal. Sci. Technol.*, 2020, **10**(21), 313–534.

48 H. Lu, Z. Zhu, H. Zhang and J. Zhu, *ACS Appl. Mater. Interfaces*, 2016, **8**(38), 25343–25352.

49 F. Huang, S. Tian, Y. Qi, E. Li, L. Zhou and Y. Qiu, *Materials*, 2020, **13**(8), 1951.

50 L. Liu, S. Li and Y. An, *Catalysts*, 2019, **9**(2), 118.

51 G. Pan, M. Xu, K. Zhou and Y. Meng, *Clays Clay Miner.*, 2019, **67**, 340–347.

52 R. Ionescu, O. D. Pavel, R. Bîrjega and R. Zăvoianu, *Catal. Lett.*, 2009, **134**, 309–317.

53 R. G. L. Gonçalves, H. M. Mendes and S. L. Bastos, *Appl. Clay Sci.*, 2020, **187**, 105477.

54 Y. H. Guan, J. Ma, D. K. Liu, Z. F. Ou, W. Zhang, X. L. Gong, Q. Fu and J. C. Crittenden, *Chem. Eng. J.*, 2018, **352**, 477–489.

55 M. E. Parolo, M. J. Avena and G. R. Pettinari, *J. Colloid Interface Sci.*, 2012, **368**(1), 420–426.

56 J. M. Wessels, W. E. Ford and W. Szymczak, *J. Phys. Chem. B*, 1998, **102**(46), 9323–9331.

57 Y. Yang, X. Hu and Y. Zhao, *J. Colloid Interface Sci.*, 2017, **495**, 68–77.

58 R. Wang, F. Chen and L. Gao, *J. Environ. Chem. Eng.*, 2022, **10**, 108361.

59 Q. R. Liu, X. G. Duan and H. Q. Sun, *J. Phys. Chem. C*, 2016, **120**(30), 16871–16878.

60 X. G. Duan, C. Su and J. Miao, *Appl. Catal., B*, 2018, **220**, 626–634.

61 H. Sun, L. Wang and F. Guo, *J. Alloys Compd.*, 2020, **900**, 163410.

62 J. Pan, L. Wang and Y. Shi, *Sep. Purif. Technol.*, 2022, **284**, 120270.

63 F. Guo, Z. Chen and X. Huang, *Sep. Purif. Technol.*, 2021, **275**, 119223.

64 W. Shi, C. Hao and Y. Shi, *Sep. Purif. Technol.*, 2023, **304**, 122337.

65 W. Shi, W. Sun and Y. Liu, *J. Hazard. Mater.*, 2022, **436**, 129141.

66 M. Shakeel, M. Arif and G. Yasin, *Appl. Catal., B*, 2019, **242**, 485–498.

67 J. Shi, X. Liu and X. Bai, *Fuel*, 2021, **306**, 121688.

68 S. He, R. Yin and Y. Chen, *Chem. Eng. J.*, 2021, **423**, 130172.

69 G. Yang, Y. A. Zhu and Y. Liang, *Appl. Surf. Sci.*, 2021, **539**, 148038.

70 S. Xin, G. Liu and X. Ma, *Appl. Catal., B*, 2021, **280**, 119386.

71 S. Xin, B. Ma and G. Liu, *J. Environ. Manage.*, 2021, **285**, 112093.

72 Y. Gao, J. Zhang and J. Zhou, *RSC Adv.*, 2020, **10**, 20991.